X-Ray and Neutron Integrated Intensity diffracted by Perfect Crystals in Transmission

D. Lambert and C. Malgrange

Laboratoire de Minéralogie-Cristallographie, Université Pierre et Marie Curie, 4, place Jussieu, 75230 Paris Cedex 05

Z. Naturforsch. **37a**, 474–484 (1982); received February 16, 1982

The integrated reflection power for perfect crystals has been measured with neutrons and X-Rays for different crystals in a wide range of absorption coefficients and values of $|\mu_h/\mu_0|$ where μ_h is the h Fourier term of the absorption coefficient. The influence of Compton effect and temperature factor is discussed. The results are compared to Kato's theoretical values.

Introduction

The value of the X-Ray integrated reflecting power for perfect crystals in transmission depends on the value of the absorption coefficient. Therefore, due to the Borrmann effect this reflecting power can be still high for high values of the product $\mu_0 t_0$ of the linear absorption coefficient μ_0 by the thickness t_0 of the crystal. The magnitude of Borrmann effect depends very much on the ratio $|\mu_h/\mu_0|$ of the modulus of the h Fourier coefficient of the absorption coefficient (for a given diffraction vector $\boldsymbol{h}$) to the absorption coefficient itself. This ratio is analyzed in detail in the first part of this paper in order to point out the influence of the position of the absorbing atoms in the unit cell and of thermal vibrations.

The integrated reflecting power for several perfect crystals with different values of $\mu_0 t_0$ and $|\mu_h/\mu_0|$ has been measured and the results are compared to theoretical values [1] (Kato, 1968) in the second part. Measurements have been performed both with X-Rays and neutrons. The agreement is very good.

We also present here some theoretical curves (calculated from Kato's formulae) giving the integrated reflection power as a function of $\mu_0 t_0$ for different values of $|\mu_h/\mu_0|$ in order to provide a quantitative estimation of the influence of this ratio on the integrated reflecting power as soon as $\mu_0 t_0$ is larger than 1.

Reprint requests to Dr. C. Malgrange, Laboratoire de Minéralogie-Cristallographie, Université Pierre et Marie Curie, 4, place Jussieu, F-75230 Paris Cedex 05, Frankreich.

1. Theoretical Value for Integrated Intensity

X-Ray dynamical theory (for reviews see [2] to [4]), shows that a plane wave $\boldsymbol{D}_0^{\mathrm{a}} \exp\{-2i\pi \boldsymbol{K}_0^{\mathrm{a}} \cdot \boldsymbol{r}\}$ incident on a perfect crystal with a given departure from Bragg angle $\Delta\theta$ on reflecting planes normal to a diffraction vector $\boldsymbol{h}$, gives rise in a transmission set up to two wavefields ($j = 1, 2$)

$$\boldsymbol{D}_j = \boldsymbol{D}_{0j} \exp\{-2i\pi \boldsymbol{K}_{0j} \cdot \boldsymbol{r}\} + \boldsymbol{D}_{hj} \exp\{-2i\pi \boldsymbol{K}_{hj} \cdot \boldsymbol{r}\}$$

propagating in the crystal with an absorption coefficient μ_{aj} given by

$$\mu_{aj} = \mu_0 \left[1 \mp \frac{\chi_{\mathrm{i}h}}{\chi_{\mathrm{i}0}} \frac{\cos \Phi}{\sqrt{1+\eta_r^2}}\right] \tag{1}$$

where the upper sign corresponds to wavefield 1 and the lower one to wavefield 2.

χ the electrical susceptibility contains a real part χ_{r} and an imaginary part χ_{i} which can be expanded as Fourier series

$$\chi = \chi_{\mathrm{r}} + i\,\chi_{\mathrm{i}},$$
$$\chi_{\mathrm{r}} = \sum_h e^{-2\pi i \boldsymbol{h}\cdot\boldsymbol{r}} \chi_{\mathrm{r}h},$$
$$\chi_{\mathrm{i}} = \sum_h e^{-2\pi i \boldsymbol{h}\cdot\boldsymbol{r}} \chi_{\mathrm{i}h}.$$

$\chi_{\mathrm{i}0}$ is related to the linear absorption coefficient μ_0 through

$$\chi_{\mathrm{i}0} = -\mu_0 \lambda/2\pi. \tag{2}$$

Φ is the phase-shift between $\chi_{\mathrm{i}h}$ and the term $\chi_{\mathrm{r}h}$ of rank h of the Fourier development of the real part χ_{r} of χ.

0340-4811 / 82 / 0500-0474 $ 01.30/0. — Please order a reprint rather than making your own copy.

η_r is the real part of η which is related to the departure from Bragg angle $\Delta\theta$ through

$$\eta = \frac{\Delta\theta \sin 2\theta - \frac{1}{2}\chi_0\left(\frac{\gamma_h}{\gamma_0} - 1\right)}{C\sqrt{\chi_h \chi_{\bar{h}}}\sqrt{|\gamma_h|/\gamma_0}}\,; \tag{3}$$

χ_h and $\chi_{\bar{h}}$ are the h and $-h$ terms of the Fourier development of the total electrical susceptibility. Then

$$\chi_h = \chi_{rh} + i\,\chi_{ih};$$

γ_0 and γ_h are the direction cosines of the incident and reflected wave vectors with respect to the normal $\boldsymbol{n}$ to the entrance surface (Figure 1 a).

Equation (1) shows that the value of μ_{aj} can be very much smaller than μ_0. Thus, the absorption of an X-Ray wave falling under Bragg incidence can be very much lower than normal absorption.

Borrmann [5] (1941, 1950) has produced the first experimental evidence for this phenomena later on called Borrmann effect or anomalous absorption.

If the crystal is rotated with an angular speed ω through a large angular range around θ_B, the total energy E per unit surface normal to the beam in the reflected direction is an integrated intensity

$$E = \int |D_h|^2\,dt = \int |D_h|^2\,d\theta/\omega\,. \tag{5}$$

The integrated reflecting power R_h^θ is then defined as the ratio of the total energy in the reflected beam to the total energy in the incident beam when the crystal is rotated of an angle equal to 1 radian. Then

$$R_h^\theta = \frac{\gamma_h}{\gamma_0}\frac{\int |D_h|^2\,d\theta}{|D_{0a}|^2}\,. \tag{6}$$

The crystal is assumed to be plane parallel and γ_h/γ_0 is the ratio of the cross sections of the reflected and incident beams (Figure 1 a).

In most experimental cases the incident beam is not a plane wave but a spherical wave $(D_0^a/r)e^{2i\pi Kr}$. Then the intensity diffracted by a motionless crystal is an integrated intensity. The integration is performed over the basis AB of Borrmann triangle (Figure 1 b).

$$P = \gamma_h \int_{l_A}^{l_B} |D_h|^2\,dl\,; \tag{7}$$

l is a coordinate along the exit surface in the plane of incidence. P is the energy per unit time in the reflected beam along a height equal to unity.

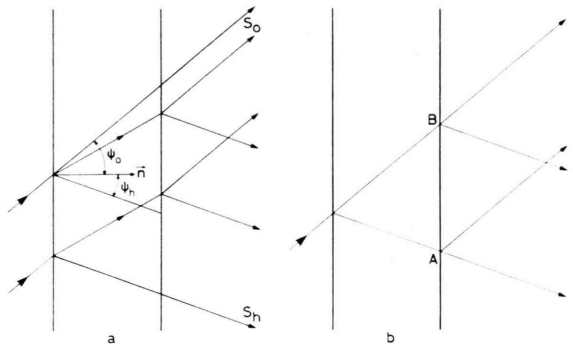

Fig. 1. Geometry of the reflected beam in a transmission set up. a) incident plane wave. One wavefield only is considered. $\gamma_0 = \cos\psi_0$; $\gamma_h = \cos\psi_h$. b) incident spherical wave.

The reflecting power is then

$$R_h^\theta = \frac{\gamma_h \int |D_h|^2\,dl}{P_0}\,, \tag{8}$$

where P_0 is the incident energy per unit time per unit glancing angle in the plane of incidence, and over a height equal to unity

$$P_0 = |D_0^a|^2/r\,. \tag{9}$$

The integrated reflecting power (6) in the case of an incident plane wave has been calculated by Ramachandran [6] (1954) and by Kato [7] (1955) independently using the small imaginary part approximation (SI) for the electrical susceptibility ($|\chi_{ih}| \ll |\chi_{rh}|$). The integrated reflecting power (8) for an incident spherical wave has been calculated by Kato [1] (1968) without any approximation on the imaginary part of χ. He has shown that in most cases his new results are equal to the previous ones within a very good approximation. Consequently, although our experiments have been performed with an incident spherical wave, we have compared our results with Kato's formulae for the integrated intensity in a case of an incident plane wave. Kato's result for R_h^θ reduces then in the symmetrical case to

$$R_h^\theta = C\frac{\Re e\sqrt{\chi_h \chi_{\bar{h}}}}{\sin 2\theta}\frac{\pi}{2}\exp\{-\mu_0 t_0/\cos\theta\} \cdot\left[\int_0^{2A} J_0(\varrho)\,d\varrho + I_0(s) - 1\right], \tag{10}$$

t_0 is the thickness of the crystal, C is the polarization factor, $2A = 2\pi t_0/\Lambda$, Λ being the extinction

length equal to

$$\frac{\lambda \cos\theta}{C\,\Re\mathrm{e}\sqrt{\chi_h \chi_{\bar{h}}}}, \quad s = 2A\,\frac{\Im\mathrm{m}\sqrt{\chi_h \chi_{\bar{h}}}}{\Re\mathrm{e}\sqrt{\chi_h \chi_{\bar{h}}}},$$

$$\chi_h = -\frac{r_e \lambda^2 F_h}{\pi V}. \tag{11}$$

If $\chi_{ih} \ll \chi_{rh}$ and for a centrosymmetric crystal

$$s = \left|\frac{\chi_{ih}}{\chi_{r0}}\right| \cos\Phi\,\frac{\mu_0 t_0}{\cos\theta} = \varepsilon H, \tag{11a}$$

where

$$\varepsilon = \left|\frac{\chi_{ih}}{\chi_{r0}}\right| \cos\Phi, \tag{12}$$

and

$$H = \mu_0 t_0/\cos\theta. \tag{13}$$

The function $W = \int_0^{2A} J_0(\varrho)\,\mathrm{d}\varrho$ where J_0 is the zero order Bessel function, oscillates around the mean value 1. These oscillations are due to interferences between wavefields 1 and 2; their amplitude decreases when the thickness of the crystal increases.

$I_0(s)$ is the modified Bessel function of zero order, equal to 1 for $s=0$ and slowly varying as far as s is small ($I_0(0.5)=1.06$). Consequently, for s small, for example $s<0.5$ R_h^θ may be approximated by

$$R_h^\theta \cong \frac{C\,\Re\mathrm{e}\sqrt{\chi_h \chi_{\bar{h}}}}{\sin 2\theta}\,\frac{\pi}{2}\exp\{-\mu_0 t_0/\cos\theta\}\,W. \tag{14}$$

On the contrary, for large value of s, for example $s>2$, $I_0(s)$ increases rapidly with s and is much larger than $W-1$ so that the oscillating term can be neglected and

$$R_h^\theta \cong \frac{C\,\Re\mathrm{e}\sqrt{\chi_h \chi_{\bar{h}}}}{\sin 2\theta}\,\frac{\pi}{2}\exp\{-\mu_0 t_0/\cos\theta\}\,I_0(s) \tag{15}$$

$$\cong \frac{C\,\Re\mathrm{e}\sqrt{\chi_h \chi_{\bar{h}}}}{\sin 2\theta}\,\frac{\pi}{2}\,e^{-s}\,I_0(s) \cdot \exp\{-\mu_0 t_0/\cos\theta\}\,(1-\varepsilon). \tag{15'}$$

Instead of R_h^θ, it is sometimes convenient to consider the proportional quantity

$$R_h^\eta = R_h^\theta \frac{\mathrm{d}\eta}{\mathrm{d}\theta} = \frac{\pi}{2}\exp\{-\mu_0 t_0/\cos\theta\}\,I_0(s). \tag{16}$$

In Fig. 2 are given several curves of $(2/\pi)\,R_h^\eta$ as a function of $H=\mu_0 t_0/\cos\theta$ for various values of the parameter ε (Equation (11)). One can notice that:

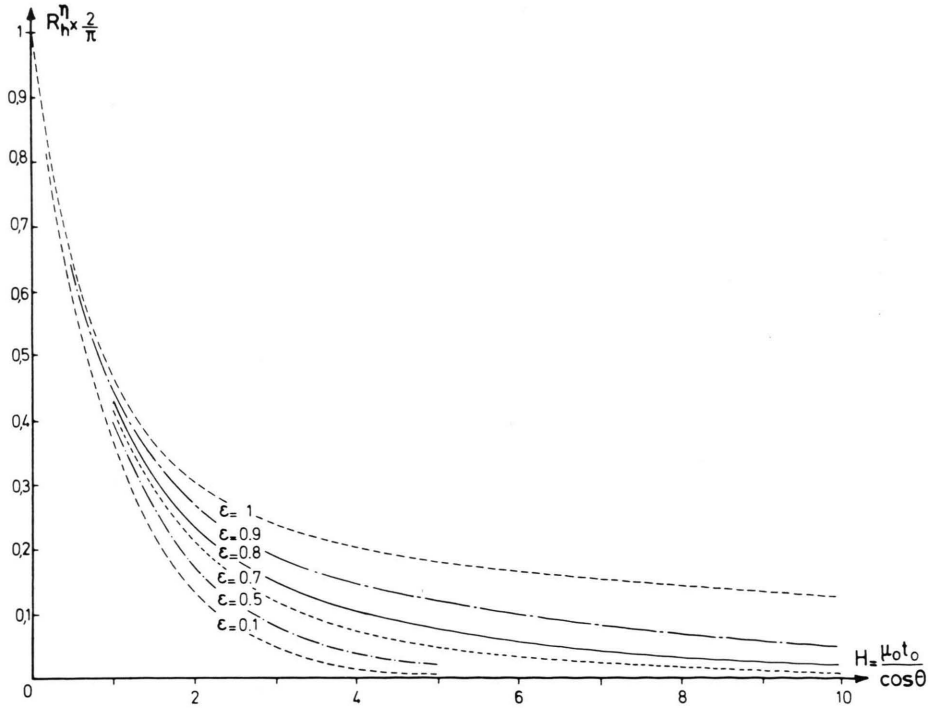

Fig. 2. Theoretical curves giving the integrated reflecting power R_h for X-Rays (or neutrons) in a transmission case as a function of $H=\mu_0 t_0/\cos\theta$ for different values of ε. The oscillating term has been neglected.

a) the largest Borrmann effect corresponds to $\varepsilon = 1$. In that case the integrated intensity first drops down rapidly as H increases and then decreases slowly keeping still quite high values for large H.

b) when ε decreases, the integrated intensity for high values of H is greatly reduced. As an example for $H = 10$ the integrated intensity is about 5 times smaller if $\varepsilon = 0.8$ than if $\varepsilon = 1$.

c) on the contrary, for H smaller than 1 the influence of ε on R_h^θ is not very important.

d) It will be shown that ε is roughly proportional to the polarization factor C. In the usual case of unpolarized X-Rays, one has to calculate separately R_h for both polarizations.

e) Let us consider expression (15′) for R_h. The tabulated values for $I_0(s)$ are given through $e^{-s} I_0(s)$ which varies from 1 for $s = 0$ to 0.46 for $s = 1$ and then decreases still more slowly ($s = 0.10$ for $s = 16$). Consequently expression (15′) shows that the most important variation for R_h^θ comes from

$$\exp\{(-\mu_0 t_0/\cos\theta)(1-\varepsilon)\}$$

which confirms the importance of the parameter $(1-\varepsilon)$.

2. Calculation of the Fourier Term χ_{ih} of the Imaginary Part of the Electrical Susceptibility

The imaginary part of the electrical susceptibility is directly proportional to the absorption coefficient (Equation 2). Then

$$\chi_{ih} = -\mu_h \lambda/2\pi \tag{17}$$

where μ_h is the h Fourier term of the linear absorption coefficient. Three phenomena contribute to the absorption: photoelectric absorption (PE), Compton scattering (C) and thermal diffuse scattering (TDS)

$$\mu = \mu_{\mathrm{PE}} + \mu_{\mathrm{C}} + \mu_{\mathrm{TDS}}. \tag{18}$$

For X-Ray wavelengths and room temperature Compton scattering and thermal diffuse scattering are much smaller than photoelectric absorption and can be neglected as a first approximation.

The theoretical derivation of μ_h for the photoelectric absorption was first presented by Molière [8] (1939) who neglected the influence of thermal vibrations in crystals. Later, Ohtsuki [9] (1964) has shown that the temperature dependance of μ_h has to be accounted for by the Debye-Waller factor a result which was confirmed experimentally by Batterman [10] (1962) and Okherse (1962) [11], Hildebrandt and Wagenfeld (1964) [12], Ling and Wagenfeld [13] (1965). Wagenfeld [14] (1966) has performed analytical and numerical calculations on photoelectric absorption cross sections for normal and anomalous absorption.

The results are the following

$$\chi_{ih} = \frac{\lambda}{2\pi}\frac{1}{V}\sum_A e^{-M_{hA}}\sigma_A(\theta_{\mathrm{B}},\lambda)\,e^{-2\pi i \boldsymbol{h}\cdot\boldsymbol{r}_A}, \tag{19}$$

where V is the volume of the unit cell, $\exp\{-M_{hA}\}$ is the Debye-Waller factor for h reflection, λ is the wavelength.

The summation has to be carried out over all atoms within the unit cell, $\boldsymbol{r}_A$ being the position vector for the A^{th} atom in the unit cell.

$\sigma_A(\theta_{\mathrm{B}},\lambda)$ is an atomic absorption cross section. It can be developped in a multipole expansion, the first terms of which are the electrical dipole, quadrupole and dipole-Octupole transitions. Their values depend on the X-Rays polarization direction.

For an electric field polarized perpendicularly to the plane of incidence one obtains

$$\sigma_{A\perp} = (\sigma_A^{\mathrm{D}} + \sigma_A^{\mathrm{D,O}}) + \sigma_A^{\mathrm{Q}}\cos 2\theta_{\mathrm{B}}. \tag{20}$$

For the electric field parallel to the plane of incidence

$$\sigma_{A\parallel} = (\sigma_A^{\mathrm{D}} + \sigma_A^{\mathrm{D,O}})\cos 2\theta_{\mathrm{B}} + \sigma_A^{\mathrm{Q}}\cos 4\theta_{\mathrm{B}}. \tag{21}$$

σ_A^{D}, $\sigma_A^{\mathrm{D,O}}$ and σ_A^{Q} are respectively the dipole, dipole-octupole and quadrupole terms. The normal absorption cross section τ_{0A} is equal to the value of $\sigma_A(\theta,\lambda)$ for $\theta = 0$

$$\tau_{0A} = \sigma_A^{\mathrm{D}} + \sigma_A^{\mathrm{D,O}} + \sigma_A^{\mathrm{Q}}. \tag{22}$$

Let us write

$$Q_A = \sigma_A^{\mathrm{Q}}/\tau_{0A}; \tag{23}$$

$\sigma_{A\perp}$ and $\sigma_{A\parallel}$ can now be written

$$\begin{aligned}\sigma_{A\perp} &= \tau_{0A}(1 - 2Q_A\sin^2\theta_{\mathrm{B}}),\\ \sigma_{A\parallel} &= \tau_{0A}\cos 2\theta_{\mathrm{B}}(1-Q_A) + Q_A\cos 4\theta_{\mathrm{B}}.\end{aligned} \tag{24}$$

Numerical values for τ_{0A} and Q_A can be found in Wagenfeld [14] (1966) and [15] Hildebrandt, Stephenson and Wagenfeld (1975). The order of magnitude of Q_A is 5.10^{-2} so that one can generally write with a good approximation

$$\sigma_\perp = \tau_0, \quad \sigma_\parallel = \tau_0\cos 2\theta.$$

Within such approximations (19) can be rewritten

$$\chi_{ih} = \frac{\lambda}{2\pi V} C \sum_A e^{-M_{hA}} \tau_{0A} e^{-2\pi i \boldsymbol{h} \cdot \boldsymbol{r}_A}, \qquad (25)$$

where τ_{0A} is the atomic photoelectric absorption cross section for atom A which depends on λ only and C is the polarization factor.

It should be noticed that apart from the polarization factor, the χ_{ih} dependance on θ_B comes from Debye-Waller factor.

In the special case of crystal containing only one kind of atoms equations (25) becomes

$$\chi_{ih} = \frac{\lambda}{2\pi V} C e^{-M_h} \tau_0 \sum_A e^{-2\pi i \boldsymbol{h} \cdot \boldsymbol{r}_A}. \qquad (26)$$

Then the importance of the geometrical factor $\sum_A e^{-2\pi i \boldsymbol{h} \cdot \boldsymbol{r}_A}$ is clear. If all the atoms emit in phase in the $K_{\boldsymbol{h}}$ direction, then $e^{-2\pi i \boldsymbol{h} \cdot \boldsymbol{r}_A}$ equals 1 for all of them and $\varepsilon = C e^{-M_h}$.

This is the case for diamond lattice crystals and even reflections, while for odd reflections

$$\varepsilon = C \frac{\sqrt{2}}{2} e^{-M_h}.$$

In the general case, ε can vary with $\boldsymbol{h}$ over a wide range because of the geometrical factor (see garnet and quartz crystals).

Let us now discuss the terms which have been neglected, namely the absorption due to Compton effect and thermal diffuse scattering, and see to what extent their contribution to $1 - \varepsilon$ can be neglected.

It has been shown theoretically by Ohtsuki [9] (1964) and Sano, Ohtaka, Ohtsuki (1969) [16] that normal and anomalous absorption coefficients for TDS, respectively called μ_0(TDS) and μ_h(TDS) are both roughly proportional to temperature and furthermore that μ_0(TDS) $- \mu_h$(TDS) is very small compared to the same quantity for photoelectric absorption (see Table 1).

It is clear from the inspection of these values for the special case of silicon crystals that the contribution of thermal diffuse scattering to $(1 - \varepsilon)$ can really be neglected.

The same authors have shown that Compton effect is porportional to the Debye-Waller factor and varies significantly with θ as expected due to the fact that not only the core electrons but all the electrons are involved in Compton scattering. Consequently, although its absolute effect remains small, Compton effect is not completely negligible as far as its contribution to $1 - \varepsilon$ is considered. An order of magnitude of μ_0 and μ_h for Compton effect and TDS is given in Table I in the special case of silicon crystals, 220 reflexion and MoKα radiation. Values estimated from Sano and al. curves are listed in the first line (the accuracy is poor because the values had to be extrapolated between wavelengths 0,5 Å and 1 Å on rather small drawings). The second line gives the values calculated by Giardini and Merlini [17] (1973) who have produced an experimental evidence for the influence of Compton effect on anomalous absorption using silicon crystals with a very high value of $\mu_0 t_0$. The final value they give for ε, 0, 954, has been used.

For crystals other than silicon, we have neglected Compton effect for two reasons:

- firstly, the accuracy on atomic temperature factor is quite poor compared to the correction which should be made to take into account Compton effect.
- secondly, since normal and anomalous absorption coefficients due to Compton scattering are proportional to Z, while photoelectric absorption increases as Z^n with $3 < n < 4$ outside absorption edges, Compton effect becomes more and more negligible as Z increases. Thus the estimation of the influence of Compton effect on ε performed above gives an upper limit for most crystalline materials.

Consequently, we have considered formula (26) as valid in every case.

Table 1. Respective contributions to normal (Index 0) and anomalous (index h) absorptions of Compton (C), thermal diffuse scattering (TDS) and photoelectric (PE) absorptions in the case of silicon and MoKα 220 reflection. S.O.O. = values from Sano, Ohtaka, and Ohtsuki. G.M. = values from Giardina and Merlini. The numerical values are given in cm^{-1}.

	$\mu_0(C)$	$\mu_h(C)$	$\Delta\mu(C)$	μ_0(TDS)	μ_h(TDS)	$\Delta\mu$(TDS)	μ_0(PE)	$\Delta\mu$(PE)
S.O.O.	0.33	0.15	0.18	0.15	0.13	0.02		
G.M.	0.316	0.156	0.160	0.180	0.158	0.022	14.11	0.497

3. Neutron Diffraction

X-Ray dynamical theory can be extended to neutron diffraction by perfect crystals. In the simple case of non magnetic crystals, Schrödinger equation for the neutron scalar wave function is formally identical to Maxwell equations for an X-Ray wave, provided the polarization factor is taken equal to 1 (M. Schlenker [18] 1975, J. Sivardière [19] (1975).

Consequently one gets in a symmetrical case

$$R_h^\theta = \frac{\lambda^2 F_h}{2\,V \sin 2\theta} \exp\{-\mu_0 t_0/\cos\theta\} \cdot \left[\int_0^{2A} J_0(\varrho)\,\mathrm{d}\varrho + I_0(s) - 1\right] \tag{27}$$

identical to (10).

Equation (11) has been used where F_h replaces $(r_e F_h)$. Since for neutrons, structure factors are calculated from scattering lengths b which correspond to the product $r_e f$ for X-Rays case ($f=$ diffusion factor, r_e: classical radius of electron).

Most elements do not absorb thermal neutrons. Then $s=0$ and the reflecting power reduces to

$$R_h^\theta = \frac{\lambda^2 F_h}{2\,V \sin 2\theta}\left[\int_0^{2A} J_0(\varrho)\,\mathrm{d}\varrho\right]. \tag{28}$$

However, some elements do absorb thermal neutrons (B, Cd, Sm, Gd). The absorption is then taken into account through the imaginary part b'' of the scattering length

$$b = b' + ib''; \tag{29}$$

b'' is related to the absorption cross section through $\sigma_a = 2\lambda b''$ (Bacon [20]) and

$$\mu_h = \sum_j e^{-M_j} \frac{\sigma_{aj}}{V} e^{-2\pi i \boldsymbol{h}\cdot\boldsymbol{r}_j} \tag{30}$$

where the summation extends over all the atoms of a unit cell.

4. X-Ray Experiments

Experiments have been carried out on several perfect crystals (silicon, quartz, gadolinium garnets) of different thickness for different diffraction vectors. The reflecting planes were always chosen perpendicular to the crystal surfaces (symmetric case). The radiation used was MoKα.

The experimental device is very simple: a fine focus (200 μm × 200 μm), a vertical slit 40 cm far from the focus. The crystal can be rotated on a vertical axis located at about 3 cm from the slit.

A stabilized X-Ray generator and a fixed slit geometry (width ~ 100 μm, height ~ a few mm) have been used in order to keep constant the incident power on the crystal for each set of measurements. The reflected intensity is measured at its peak value with a scintillation counter. The intensity which is measured that way is an integrated intensity because the incident beam is divergent. Its divergence θ_i is given by the angle subtended by the source at the slit location, about $5 \cdot 10^{-4}$ radians. This value is much larger than the intrinsic width of the rocking curves and large enough to be sure that in each case the whole spectral width $\Delta\lambda$ for MoKα_1 radiation is in reflection position (this is schematically shown in Fig. 3 with a DuMond diagram). However, this value is small enough to separate Kα_1 and Kα_2 radiations. With such a simple device we cannot obtain the reflecting power because we have no measure of the incident power, but for each set of measurements this power is kept constant.

In order to compare experimental and theoretical results we have proceeded in two different ways

- either, as in paragraph a) by choosing one result as a reference supposed to agree with theory and then comparing the other experimental results to theoretical ones
- or, more generally, by calculating the ratio between the measured intensity and the theoretical reflecting power and checking the constance of this ratio within experimental errors and theoretical approximations.

Let us notice that the incident X-Ray beam is unpolarized and the reflecting power is then equal to

$$R_h^\theta = \frac{\pi}{4}\frac{\mathrm{Re}\sqrt{\chi_h \chi_{\bar{h}}}}{\sin 2\theta} \exp\{-\mu_0 t_0/\cos\theta\} \cdot \left[\left(\int_0^{2A_\perp} J_0(\varrho)\,\mathrm{d}\varrho + I_0(s_\perp) - 1\right) + \cos 2\theta\left(\int_0^{2A_\parallel} J_0(\varrho)\,\mathrm{d}\varrho + I_0(s_\parallel) - 1\right)\right]. \tag{31}$$

$A_\perp$ and $A_\parallel$, $s_\perp$ and $s_\parallel$ are the respective values of A and s for perpendicular polarization ($C=1$) and parallel polarization ($C=\cos 2\theta$).

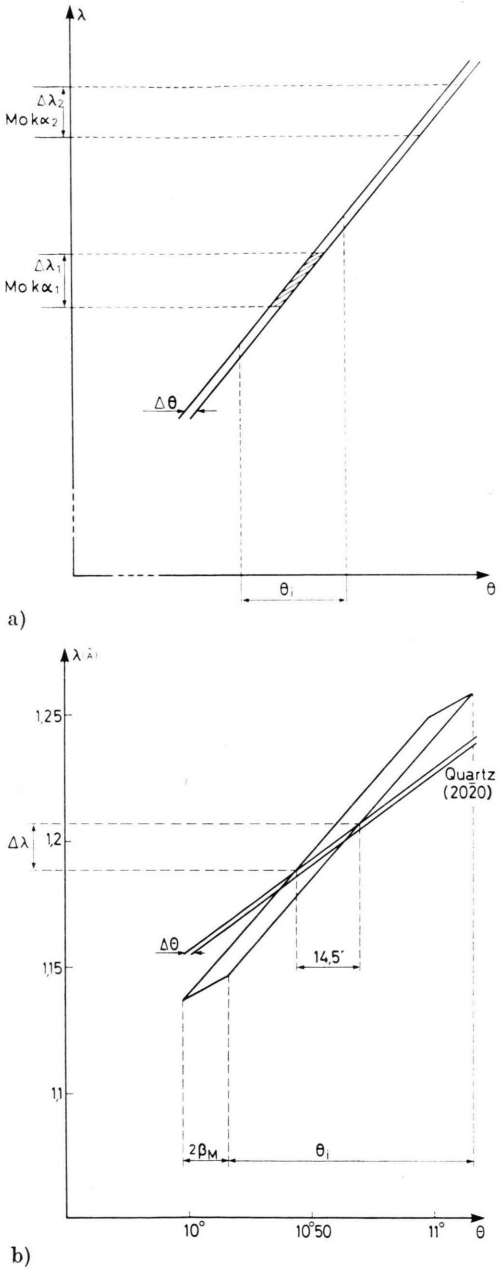

Fig. 3. Du Mond diagrams. a) X-Ray case: monochromatic radiation. $\Delta\lambda_1$ is the spectral width of MoKα_1 line. $\Delta\theta$ is the angular width of the reflection intrinsic rocking curve. θ_i is the horizontal divergence of the incident beam. b) Neutron case: white incident beam and a monochromator. β_M is the monochromator mosaicity.

a) Silicon Crystals

Four perfect silicon crystals have been used with respective thickness equal to 665 μm, 700 μm, 2.45 mm and 3.90 mm. Their faces were (111) and reflected intensities for symmetric 220, 440 reflections have been measured.

For all these thicknesses, Pendellösung oscillations can be neglected and

$$R_h^\theta = \frac{\lambda^2 F_h r_e}{4 V \sin 2\theta} \exp\{-\mu_0 t_0/\cos\theta\} \cdot [I_0(s_\perp) + \cos 2\theta\, I_0(s_\parallel)] \quad (32)$$

the values of $s_\parallel$ and $s_\perp$ have been calculated using $\mu = 14.6\ \text{cm}^{-1}$ from Hildebrandt et al. [22] (1973). $\varepsilon_{\perp(220)}$ was taken equal to 0.954 as explained above. For $\varepsilon_{\perp(440)}$, Compton effect has not been calculated so that we have neglected it and we have used $e^{-M} = 0.875$ from Hildebrandt, Stephenson and Wagenfeld [22] (1973).

The results are plotted in Fig. 4 as a function of $H = \mu_0 t_0/\cos\theta$ and compared to the theoretical curves for each reflexion. The value of the intensity diffracted by the 2.45 mm thick crystal for 220 reflexion has been taken as a reference. The scale is different for the two curves in order to normalize to 1 the intensities for zero thickness. The agreement between experimental and theoretical values is very good.

b) Quartz Crystals

Measurements have been made on two natural quartz crystals with respective thicknesses equal to 200 μm and 1 mm. Lang topographs of these two crystals have been made. The thinner crystal presented only surface defects which have been eliminated by etching; the thicker one although presenting some defects, contained enough perfect areas to perform the measurements.

Diffracted intensities have been measured for symmetric $10\bar{1}0$, $20\bar{2}0$, $30\bar{3}0$ reflections. Structure factor, anisotropic temperature factors and lattice parameters are taken from Zachariasen and Plettinger [23] (1965). The corresponding calculated values of $\varepsilon_\perp$ are given in Table 2.

It is interesting to notice the low $\varepsilon_\perp$ values for $10\bar{1}0$ and $30\bar{3}0$ reflections.

In the same table are given the values of the Pendellösung period in order to show that for the 200 μm crystal, Pendellösung effect has to be taken into account through the oscillating W term.

The measured integrated reflected intensity and its ratio to the theoretical integrated reflecting power are given in Table 3. This ratio is constant within a 2.4% statistical error.

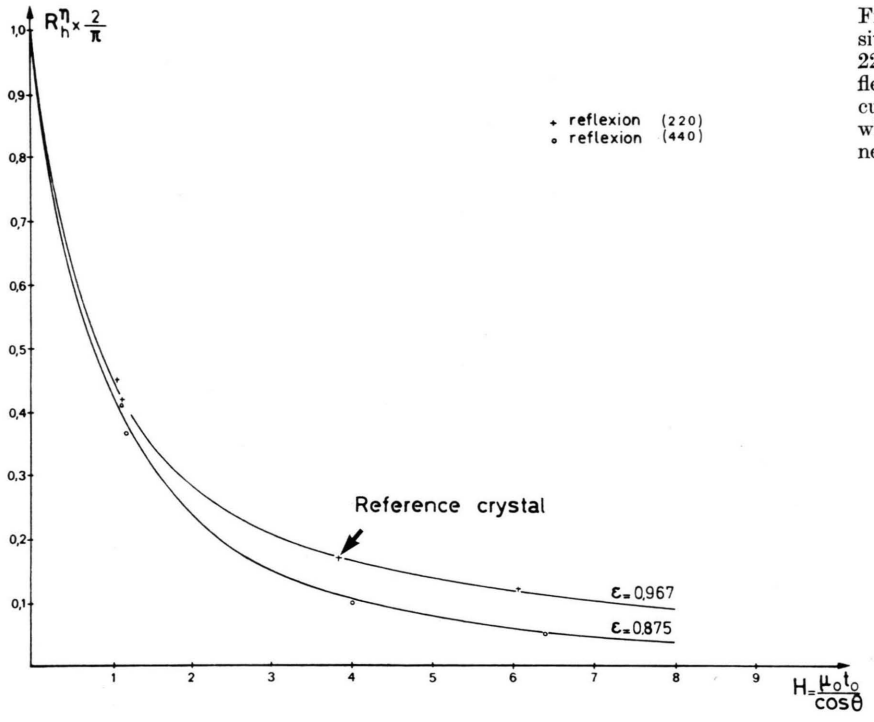

Fig. 4. Integrated reflected intensities for silicon crystals. + MoKα_1 220 reflection, ● MoKα_1 440 reflection. Theoretical curves are calculated from Kato's formulae where the oscillating term has been neglected.

c) Gadolinium Garnet Crystals: $Gd_3Ga_5O_{12}$ or GGG

These crystals have been chosen because of their high value of the absorption coefficient for neutrons as well as for X-Rays. X-Ray topographs of a (111) sample have shown that this crystal was dislocation free but contained growth bands, the contrast of which depends on the diffraction vector. For the symmetric $8\bar{8}0$ reflection the contrast is very faint and the crystal can be considered as quite perfect.

The sample was split into two parts which were thinned down to thicknesses respectively equal to 400 μm and 320 μm.

The atomic absorption coefficients for Gd, Ga and O atoms for MoKα radiation are given in International tables for X-Ray Crystallography and lead to a linear absorption coefficient equal to 3.47/100 μm.

The GGG structure (space group Ia3d or O_h^{10}) is such that the significantly absorbing atoms Gd and Ga occupy positions for which coordinates are multiple of 1/8. For diffraction vectors with h, k, l values multiple of 8, each term $e^{-2\pi i \boldsymbol{h}\cdot\boldsymbol{r}_j}$ in the

Tables 2. Values of different parameters which enter in integrated reflecting power for quartz crystals and MoKα_1 radiation.

	$10\bar{1}0$	$20\bar{2}0$	$30\bar{3}0$
θ_B	4.79°	9.62°	14.51°
F_h	16.10	17.10	8.25
$\varepsilon_\perp$	0.204	0.744	0.191
$\Lambda_\perp$ (m)	109.7	102.1	207.7
$\Lambda_\parallel$ (m)	111.2	108.1	237.5

Crystal	Reflexion	$H = \frac{\mu_0 t_0}{\cos\theta}$	$R_h^\theta \times 10^5$	I_{exp} $\times 10^{-4}$ c/s	I_{exp}/R_h^θ $\times 10^{-9}$ c/s
Si 665 μm	220	0.98	0.36	63	175
Si 665 μm	440	1.04	0.097	16.5	170
Quartz 1 mm	$10\bar{1}0$	0.973	0.232	42	181
Quartz 1 mm	$20\bar{2}0$	0.984	0.1415	25	177
Quartz 1 mm	$30\bar{3}0$	1.00	0.036	6	167
Quartz 200 μm	$10\bar{1}0$	0.195	0.388	68	175
Quartz 200 μm	$20\bar{2}0$	0.197	0.192	33	172
Quartz 200 μm	$30\bar{3}0$	0.200	0.056	9.5	170

Table 3. Comparison of experimental and theoretical values (I_{exp} and R_h^θ respectively) for the X-ray integrated reflecting power of different silicon and quartz crystals. The ration I_{exp}/R_h^θ in the last column is constant within a 2.4% statistical error.

Table 4. Comparison of experimental and theoretical values, I_{exp} and R_h^θ, for the X-Ray integrated reflecting power of different silicon and garnet crystals. Theoretical values for GGG crystals have been calculated for two different values for ε which is not well known because of temperature factors. The ratio I_{exp}/R_h^θ for GGG crystals is equal to the values obtained for silicon crystals if ε is equal to 0.955.

	Reflexion	$H = \frac{\mu_0 t_0}{\cos\theta}$	$R_h^\theta \times 10^6$	I_{exp} c/s	$I_{exp}/R_{h\theta} \times 10^{-10}$ c/s
Si 700 μm	220	1.04	3.5	70 000	2
Si 3.9 mm	220	5.79	0.95	18 000	1.9
GGG 320 μm	$8\bar{8}0$	12.21	0.24 with $\varepsilon = 0.93$ 0.315 with $\varepsilon = 0.955$	6 000	2.5 ($\varepsilon = 0.93$) 1.9 ($\varepsilon = 0.955$)
GGG 400 μm	$8\bar{8}0$	15.27	0.175 with $\varepsilon = 0.93$ 0.235 with $\varepsilon = 0.955$	4 800	2.7 ($\varepsilon = 0.93$) 2.0 ($\varepsilon = 0.955$)

sum (25) is equal to 1 for Gd and Ga atoms so that $\varepsilon \sim C \sum_j e^{-M_j}$. It is impossible to find accurate values for temperature factors firstly because structural work has been done on magnetic garnets only and secondly because even on these garnets "the values obtained should be considered only as rather rough approximations" (Weidenborner [24] 1961). If one uses the values obtained in this paper for Gd, Fe garnets, $B_{Gd} = 0.25$ Å^2 and $B_{Ga} = 0.49$ Å^2, one finds $\varepsilon = 0.93$.

The measured integrated intensities I_{exp} and their ratio to theoretical values of R_h^θ are given in Table 4. This ratio is compared to the values obtained previously with different silicon crystals and different reflexions. If the value of ε is taken equal to 0.93 the agreement between experiment and theory is not very good for GGG crystals. For such quite high values of μd (here 11.1 and 13.9), the theoretical values of the integrated reflecting power are very sensitive to variations of ε. Changing the ε value to 0.955 gives then a good agreement between experiment and theory.

5. Neutron Experiments

Neutron experiments were performed with a vertical double axis spectrometer in canal H9 of EL3 reactor in Saclay. The white neutron beam is monochromatized with a Ge crystal (mosaicity of the order of 5 minutes) and 111 reflection. The monochromator was adjusted to give a wavelength equal to 1.2 Å.

The vertical and horizontal divergence of the incident beam was of the order of 1 degree. The vertical angular width of the beam reflected by the samples was kept constant for all the measurements by putting a slit limiting the height of the beam to a value smaller than the height of the crystals.

The horizontal angular width and the spectral width of the beam reflected by the sample in a parallel adjustment both depend on the mosaicity of the monochromator and on relative Bragg angles for the two crystals. The magnitude of this horizontal width and the corresponding spectral width $\Delta\lambda$ can be easily evaluated with the help of DuMond diagrams [25]. The neutron diffracted intensity is then proportional to $R_h^\theta \times \Delta\lambda$ which will be called here global reflecting power P_h^θ.

Four crystals have been tested: two silicon crystals, 2.45 mm and 3.90 mm thick, adjusted for 220 reflection, the 200 μm quartz crystal for $20\bar{2}0$ reflexion and the 320 μm GGG crystal for $8\bar{8}0$ reflection. DuMond diagram for quartz crystal and $20\bar{2}0$ reflexion is shown on Fig. 3b as an example.

Table 5 gives structure factors, absorption $\mu_0 t_0/\cos\theta$ Pendellösung lengths Λ, spectral widths $\Delta\lambda$ in the four different cases.

Silicon and quartz crystals do not absorb thermal neutrons so that according to formula (28)

$$P_h^\theta = \Delta\lambda \frac{\lambda^2 F_h}{2V \sin 2\theta} \int_0^{2A} J_0(\varrho)\, d\varrho .$$

Table 5. Structure factors F_h, Pendellösung length Λ and spectral width of the beam $\Delta\lambda$ for different crystals for 1.2 Å neutrons monochromatized by a 111 reflection on a Germanium crystal.

Crystal	Silicon	Quartz	GGG
Reflection	220	$20\bar{2}0$	$8\bar{8}0$
Bragg angle	18.2°	16.3°	33.25°
$F_h \times 10^{12}$ cm	3.26	0.65	56.4
Λ (μm)	122.5	436.5	73.7
$\Delta\lambda \times 10^3$ Å	12.7	17.2	4.25

On the contrary, owing to the gadolinium nuclei, GGG crystals strongly absorb thermal neutrons. Pendellösung oscillations can now be neglected and

$$P_h^\theta = \Delta\lambda \frac{\lambda^2 F_h}{2V \sin 2\theta} \exp\{-\mu_0 t_0/\cos\theta\} I_0(s).$$

Natural gadolinium contains two isotopes Gd^{155} and Gd^{157} which both absorb thermal neutrons. The resonance takes p'ace for wavelengths respectively equal to 1.75 Å and 1.614 Å. We have calculated the neutron absorption cross sections from Breit-Wigner equations [20] (Bacon) using the resonant parameters given in Neutron Cross sections BNL 325. The linear absorption coefficient is then 25.5 mm^{-1} for 1.2 Å wavelength. As we have mentioned above the value of the integrated reflected intensity is very sensitive to the thermal parameter. For the e^{-M} factor of Gd atoms we have taken the value 0.97 coherent with the best fitting value for X-Rays, 0.955, which takes into account heavy Gd and lighter Ga atoms. Neutron diffracted intensities were measured with a BF_3 counter. Experimental results, I_{exp}, and theoretical values for the global reflecting power P_h^θ are given in Table 6. In the last column the ratio I_{exp}/P_h^θ is given and stays quite constant which means a good agreement between theory and experiments if one keeps in mind the different possible causes of error (uncertainty in e^{-M} values, distribution of the incident beam considered as rectangular etc. ...). On the contrary the value of the same ratio in the case of a non perfect $GdAlO_3$ crystal is quite different, a result which is discussed below.

Table 6. Comparison of experimental and theoretical values of the neutron reflecting power for different crystals. The comparison is made through the ratio of the experimental I_{exp} and theoretical results P_h which is constant for perfect crystals.

Crystal	Reflexion	$H = \frac{\mu_0 t_0}{\cos\theta}$	P_h^θ (Å) $\times 10^9$	I_{exp} (c/s)	I_{exp}/P_h^θ $\times 10^8$
Si 2.45 mm	220	0	31.4	13.8	4.4
Si 3.90 mm	220	0	31.4	14.3	4.5
Quartz	$20\bar{2}0$	0	18.8	9	4.8
GGG 320 μm	$8\bar{8}0$	9.6	0.99	0.5	5.0
non perfect $GdAlO_3$	220	10.1	5.15	1	1.9

Conclusion

It has been shown here that a good evaluation of the integrated reflecting power by perfect crystals in transmission could be easily done by using Kato's formula which is very dependent on the ratio.

$$\varepsilon = |\chi_{ih}/\chi_{i0}| \cos\Phi.$$

We have shown that, as a first approximation, the influence on ε of Compton effect and thermal diffuse scattering could be neglected with respect to photoelectric absorption more especially as, generally, Debye-Waller temperature factor is not known with a high accuracy. As the sensitivity to temperature factors is shown to be in some cases very high, such measurements of the integrated reflection power could be used to measure them.

The ε dependence on the geometrical factor has been pointed out and examples have been given where ε varies over a wide range depending on atomic positions in the unit cell and on the diffraction vector. These examples correspond to the perfect crystals which were available to us and on which measurements of integrated reflected power have been performed with X-Rays and neutrons as well. The results are in good agreement with Kato's formula in both cases.

The same measurements have been performed on a $GdAlO_3$ crystal which contains a dislocation network giving thin white images on an X-Ray topograph. The X-Ray integrated reflexion power was nearly equal to the perfect crystal value. On the contrary the value for the neutron integrated reflexion power was half that expected for the perfect crystal (see Table 6); the explanation is the following: owing mainly to smaller structure factors the width of neutron topographic images is larger than for X-Rays; consequently, a given density of dislocations gives larger white images with neutrons and then a decrease in the reflected intensity.

Acknowledgements

We are greatly indebted to H. L. Glass (Rockwell, USA) who kindly supplied the Gadolinium Garnet crystal. We express our thanks to M. Englander for his cooperation in using neutron facilities. We are very grateful towards M. Schlenker (Laboratoire de Magnétisme, Grenoble) for valuable suggestions and discussions.

[1] N. Kato, J. Appl. Physics **39**, 2225 (1968).
[2] A. Authier, Section topography in X-Ray Optics ed. by H. J. Queisser, Springer Verlag, Berlin 1977.
[3] B. W. Batterman and H. Cole, Rev. Mod. Physics **36**, 681 (1964).
[4] L. V. Azaroff, R. Kaplow, N. Kato, R. J. Weiss, A. J. C. Wilson, and R. A. Young, X-Ray Diffraction. McGraw-Hill, New-York 1974.
[5] G. Borrmann, Z. Physik **127**, 297 (1950).
[6] G. N. Ramachandran, Proc. Indian Acad. Sci. **A39**, 65 (1954).
[7] N. Kato, J. Phys. Soc. Japan **10**, 46 (1955).
[8] G. Moliere, Ann. Physik **35**, 272 (1939).
[9] Y. M. Ohtsuki, J. Phys. Soc. Japan **19**, 2285 (1964).
[10] B. W. Batterman, Phys. Rev. **127**, 686 (1962).
[11] B. Okherse, Philips. Res. Rept. **17**, 464 (1962).
[12] G. Hildebrandt and H. Wagenfeld, Acta Cryst. **16**, A160 (1964).
[13] D. Ling and H. Wagenfeld, Phys. Letters **15**, 8 (1965).
[14] H. Wagenfeld, Phys. Rev. **144**, 1, 216 (1966).
[15] G. Hildebrandt, J. D. Stephenson, and H. Wagenfeld. Z. Naturforsch. **30a**, 697 (1975).
[16] H. Sano, K. Ohtaka, and Y. H. Ohtsuki, J. Phys. Soc. Japan **27**, 1254 (1969).
[17] M. D. Giardina and A. Merlini, Z. Naturforsch. **28a**, 1360 (1973).
[18] M. Schlenker, International Summer School on X-Ray Dynamical Theory and Topography, Limoges, France 1975, unpublished.
[19] J. Sivardiere, Acta Cryst. **A31**, 340 (1975).
[20] G. E. Bacon, Neutron Diffraction, Clarendon Press, London 1975, 3rd edition.
[21] P. J. E. Aldred and M. Hart, Proc. Roy. Soc. Lond. **A332**, 223 (1973).
[22] G. Hildebrandt, J. D. Stephenson, and H. Wagenfeld, Z. Naturforsch. **28a**, 588 (1973).
[23] W. H. Zachariasen and H. A. Plettinger, Acta Cryst. **18**, 710 (1965).
[24] J. E. Weidenborner, Acta Cryst. **14**, 1051 (1961).
[25] J. W. M. Du Mond, Phys. Rev. **52**, 871 (1937).